Adsorption of NH₃ and NO₂ Molecules on Sn-Doped and Undoped ZnO (101) Surfaces Using Density Functional Theory

Ratshilumela S. Dima [1,2,*], David Magolego Tshwane [3,4], Katekani Shingange [5], Rosinah Modiba [3], Nnditshedzeni E. Maluta [2,4] and Rapela R. Maphanga [1,4]

1   Next Generation Enterprises and Institutions Cluster, Council for Scientific and Industrial Research, Pretoria 0001, South Africa
2   Department of Physics, University of Venda, Thohoyandou 0950, South Africa
3   Advanced Materials Engineering, Future Production: Manufacturing, Council for Scientific and Industrial Research, Pretoria 0001, South Africa
4   National Institute for Theoretical and Computational Sciences (NITheCS), Gauteng 2000, South Africa
5   DST/CSIR National Centre for Nanostructured Materials, Council for Scientific and Industrial Research, Pretoria 0001, South Africa
*   Correspondence: sdima@csir.co.za

Abstract: The adsorption and interaction mechanisms of gaseous molecules on ZnO surfaces have received considerable attention because of their technological applications in gas sensing. The adsorption behavior of NH₃ and NO₂ molecules on undoped and Sn-doped ZnO (101) surfaces was investigated using density functional theory. The current findings revealed that both molecules adsorb via chemisorption rather than physisorption, with all the adsorption energy values found to be negative. The calculated adsorption energy revealed that the adsorption of the NH₃ molecule on the bare ZnO surface is more energetically favorable than the adsorption of the NO₂ molecule. However, a stable adsorption configuration was discovered for the NO₂ molecule on the surface of the Sn-doped ZnO surface. Furthermore, the adsorption on the undoped surface increased the work function, while the adsorption on the doped surface decreased. The charge density redistribution showed charge accumulation and depletion on both adsorbent and adsorbate. In addition, the density of states and band structures were studied to investigate the electronic behavior of NH₃ and NO₂ molecules adsorbed on undoped and Sn-doped ZnO (101) surfaces.

Keywords: density functional theory; adsorption energy; gas sensors; doped ZnO

1. Introduction

Sensors assist in identifying the different types of pertinent information in the immediate environment and translate the obtained information into an information output such as an electrical signal. Gas sensors are among the common kinds of sensors and are generally used for the identification and detection of harmful or toxic gases. For example, ammonia (NH₃) is commonly used in industries such as cleaning and manufacturing chemicals, and as a refrigerant; exposure to NH₃ at 25 ppm or higher concentrations can cause irritation of the lung, skin, and eyes [1]. Nitrogen dioxide (NO₂) is an important material for the synthesis of nitric acid that is used in the production of fertilizers and explosives; however, exposure to NO₂ at a concentration greater than 1ppm can damage the respiration system [2]. In addition to these examples, gas sensors play very important roles in the food industry, automotive industry, and many other fields [3]. Therefore, it is important to understand their role in the respective applications and the mechanisms behind their performance.

To date, different gas sensors based on semiconductor metal oxide (SMO), including SnO₂, TiO₂, ZnO, and WO₃, have shown outstanding gas detection performance when in contact with oxidizing or reducing gases [4–6]. SMO materials operate based on changes in

the electrical resistance of the sensing material upon contact with the analyte gas. The type of sensing mechanism depends on the type of material (p/n type), the type of gas (oxidizing/reducing), and environmental conditions such as temperature [7].

Among SMO-material-based sensors, ZnO-based gas sensors are considered to be the most potential candidates because of their physical, chemical, optical, and electrical properties. Extensive experimental research on the sensing performance of ZnO-based sensors has been reported on the sensing capabilities of CO [8], NH_3 [9], NO_2 [10], ethanol [11], and other gases [12,13]. However, ZnO has challenges, such as high-power consumption and poor selectivity, thus hindering its practical application. To overcome these challenges, strategic approaches such as noble metal incorporation [14,15], doping [16,17], and heterostructures [18,19] have been developed. Of the mentioned strategies, doping has been found to enhance the sensing performance of ZnO because of the microstructural changes induced by the dopant. For example, Patil et al. [20] observed enhanced NO_2 sensing performance for Al-doped ZnO nanorods [20]. Zhao et al. [21] reported on the enhanced ethanol sensing capabilities induced by the doping of ZnO nanowires with rare earth elements (Ce, Eu, and Er) [21]. These reports have also confirmed that the gas adsorption mechanisms that occur on the surface of the sensing material play vital roles in gas sensing.

Previously, the adsorption stability of NH_3, NO, and Co molecules on bare and (Ag, Au)-doped ZnO monolayers has been investigated using density functional theory (DFT) [22]. The adsorption stability of NH_3 molecules on a bare ZnO surface was reported to be higher. More importantly, it was stated that (Ag, Au) dopants improve adsorption strength, except for the NH_3 molecule. Liangruksa et al. reported the use of the first-principle approach to investigate the adsorption of gases CH_4, N_2O, NO, NH_3, and CO on a Pd-modified ZnO (0001) surface [23]. The adsorption stability of NH_3 gas was reported to be the most stable, compared with other gases, with an adsorption energy value of -1.06 eV. This previous study established an adsorption strength on the modified ZnO surface, indicating a significant sensitivity to these gases [23].

Therefore, keeping this in mind, we first investigated the sensing properties of pure and tin (Sn)-doped ZnO using DFT calculations. Doping ZnO with Sn can modify the structural, electrical, and optical properties of ZnO, which in turn can influence the gas sensing performance. In this work, the chemisorption and physisorption mechanisms were systematically considered, wherein the adsorption energy, work function, electronic properties, and charge density redistribution were calculated. Understanding the adsorption stability strength and electronic properties of NH_3 and NO_2 molecules on ZnO surfaces will elucidate their fundamental gas sensing mechanisms. Other works on the absorption of NO_2 and NH_3 have been reported before for other SMOs; for example, Prades et al. [24] reported on the adsorption of NO_2 and NO on a SnO_2 (110) surface [24]. The results showed that the NO_2 adsorption strength decreased as the surface area decreased. Furthermore, the bridging oxygen site was discovered to be the most stable adsorption site for both NO and NO_2 molecules. The interaction of NH_3 gas with the surface of kaolinite revealed a greater adsorption capacity at the hollow position than at the top and bridge positions via the N atom site [25]. The stable adsorption configuration of NH_3 was observed by Zhu et al. [26] on a Mn^{4+} site, whereas the adsorption energy of the NO molecule was highest at the O top site of the MnO_2 (110) surface through nitrogen coordination [26].

In this work, using the most stable ZnO (101) surface [27], we studied the changes in electronic band structure upon its exposure to a reducing gas compound, NH_3, and an oxidizing gas compound, NO_2. Our goal was to theoretically interpret the gas sensing mechanism involving the ZnO surface in the presence of reducing and oxidizing gas compounds and to also explain how Sn doping influences these mechanisms.

2. Materials and Methods

All the density functional theory calculations were carried out using a Cambridge Serial Total Energy Package (CASTEP) code [28], as implemented in Material Studio Software (MS2020) of BIOVIA Inc, USA, California, San Diego. The Perdew–Burke–Ernzerhof

(PBE) exchange–correlation functional was employed within a generalized gradient approximation (GGA) [29]. All the calculations were optimized with the convergence tolerance accuracy and maximum force of 10^{-5} eV/atom and 0.03 eV/Å, respectively. We used a convergence plane-wave cutoff energy value of 500 eV and k-points gride of $6 \times 2 \times 5$ using the Monkhorst–Pack approach [30] for surface and adsorption calculations. During geometry optimization, the limited-memory Broyden–Fetcher–Goldfarb–Shanno minimization scheme algorithm was used. The surface models were created from the optimized bulk structure of the ZnO crystal with a space group F-43m and lattice parameter a = b = c = 4.625 Å. The surface models were generated to have symmetric top and bottom layers to avoid dipole effects. The surface slabs were represented by five atomic layers separated by a vacuum region of 25 Å to avoid self-interaction. The inner layers were fixed, and the rest of the system was allowed to relax during structural optimization. To describe the reaction of gas molecules with the doped and undoped surfaces, the molecules were in position 2 Å on top of the surface. The adsorption energy strength was calculated using the following expression:

$$E_{ads} = E_{mol\text{-}surf} - (E_{surf} + E_{mol}) \tag{1}$$

where $E_{mol\text{-}Surf}$, E_{surf}, and E_{mol} describe the total energy values of the combined molecule–surface structure, the doped or undoped surface, and the free molecule, respectively. Both NH_3 and NO_2 molecules were placed above Zn and the dopant (Sn) on the surface, and full geometry optimization was performed.

## 3. Results and Discussion

3.1. Structural Analysis

Figure 1 depicts the atomic surface slabs for ZnO (101) and Sn-ZnO (101) to describe the surface plane. The surface slabs were constrained to have 5 atomic layers with 20 atoms. The equilibrium distance between the nearest surface layer ranged from 1.3 to 1.5 Å, with bond lengths $d_{Zn\text{-}O}$ (1.871 Å) and $d_{Sn\text{-}O}$ (2.083 Å).
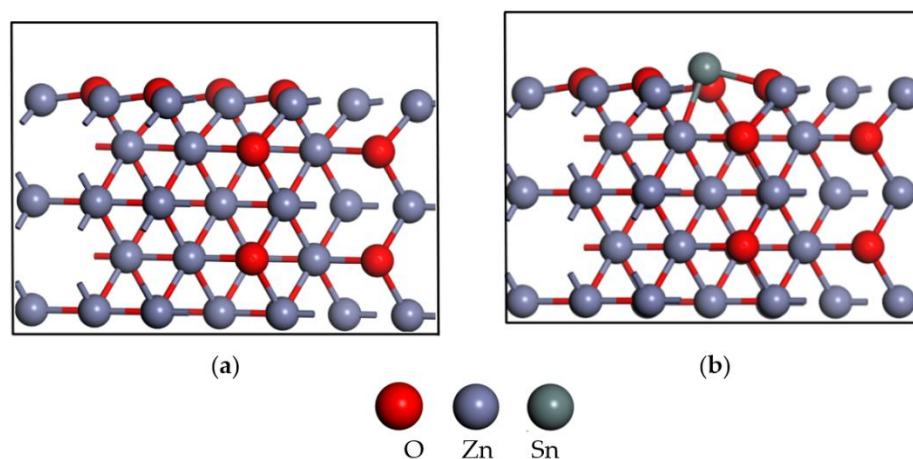
Figure 1. Optimized atomic side-view of (**a**) pure ZnO (101) surface and (**b**) Sn-doped ZnO (101) surface.

In order to investigate the effects of NH_3 and NO_2 exposure, both molecules were placed above Zn and the dopant (Sn) on the ZnO (101) surface, and full geometry optimization was performed. Figure 2 presents the optimized atomic structure of NH_3 and NO_2 molecule adsorption on the doped and undoped surfaces, namely (a) NH_3/ZnO (101), (b) NO_2/ZnO (101), (c) NH_3/Sn-ZnO (101), (d) NO_2/Sn-ZnO (101), (e) chemisorption NH_3/Sn-ZnO (101), and (f) chemisorption NO_2/ Sn-ZnO (101) surfaces. The adsorption interaction configuration of both molecules with pure and doped ZnO (101) surfaces led by N atom bonding. It is worth noting that the equilibrium bond distance between the N atom of the molecule and the surface differed. The bond distance ($d_{N\text{-}Sn}$, Å) for NH_3 adsorption was found to be 2.785 Å, which was larger than $d_{N\text{-}Zn}$, with 2.163 Å. A similar observation

was also noted on the NO_2 molecule adsorption, where the bond distance of d_{N-Zn} was smaller (2.361 Å) than $d_{N-Sn} = 2.497$ Å.
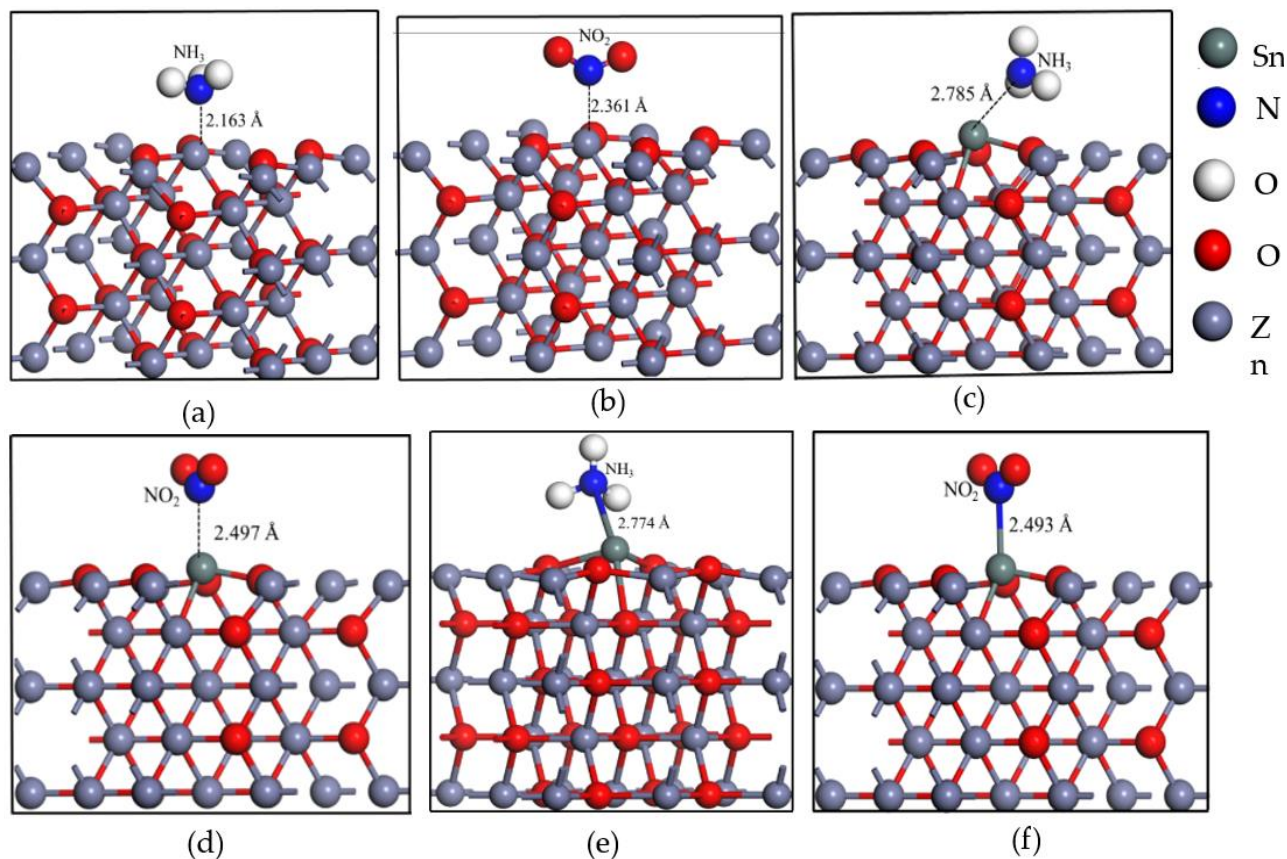
Figure 2. Optimized atomic structure of NH_3 and NO_2 molecule adsorption on doped and undoped surfaces: (**a**) NH_3/ZnO (101), (**b**) NO_2/ZnO (101), (**c**) NH_3/Sn-ZnO (101), (**d**) NO_2/Sn-ZnO (101), (**e**) chemisorption NH_3/Sn-ZnO (101), and (**f**) chemisorption NO_2/ Sn-ZnO (101) surface.

3.2. Adsorption Energy

The adsorption mechanism and exposure of the NH_3 and NO_2 gaseous molecules on the surface were investigated by calculating the adsorption energy using Equation 1. Table 1 presents the adsorption energy rates (E_{ads}, eV) and equilibrium bond distance (d, Å). In this work, both chemisorption and physisorption approaches were considered to investigate the nature of adsorption. Generally, physisorption is adsorption without bonding, while chemisorption is adsorption with bonding. Upon a comparison of the adsorption energy, it was found that all the adsorption energy rates were negative, indicating thermodynamic stability. Strong adsorption was distinguished by the greatest negative value of adsorption energy. $E_{ads} < 0$ implies that the adsorption process occurred spontaneously due to attractive interaction and exothermic process. The chemisorption process was completed by placing the molecules in different positions (1 Å and 2 Å) above the surface. It was found that the calculated adsorption energy rates at 1 Å positioning were more preferential than those at 2 Å, suggesting a stronger interaction.

Table 1. Calculated adsorption energy values ($E_{ads.}$, eV) of NH_3 and NO_2 molecules on doped and undoped ZnO (101) surfaces and atomic bond distance (d_{N-Zn}, d_{N-Sn}, Å) for the nearest atoms.

System	(dN-Zn, dN-Sn, Å)	Eads (eV)		
		Physisorption		Chemisorption
		1 Å	2 Å	Å
NH_3/ZnO (101)	2.163–2.162	−1.042	−0.746	−0.746
NO_2/ZnO (101)	2.361–2.360	−0.354	−0.280	−0.279
NH_3/Sn-ZnO (101)	2.785–3.148	−0.339	−0.187	−0.357
NO_2/Sn-ZnO (101)	2.493–2.522	−1.105	−0.436	−0.438

In addition, it was clearly observed with the adsorption energy results that the Sn-doped ZnO surface exhibited an interaction of the NO_2 molecule in both physisorption and chemisorption processes; however, the adsorption of NH_3 remained similar. The calculated adsorption energy of the NH_3 molecule on the ZnO (101) surface was −0.746 eV, which was negatively larger than the E_{ads} (−0.279 eV) of the NO_2 adsorption. Generally, a larger negative value of the adsorption energy suggests a stable configuration and stronger interaction. This implies that the NH_3 molecule adsorption was more favorable than the adsorption of NO_2 on the ZnO (101) surface. Furthermore, this indicates a weak interaction in the NO_2/ZnO (101) surface due to the large bond distance (d_{N-Zn} = 2.785 Å).

A significant adsorption energy value was observed on the doped ZnO (101) surface. The chemisorption and physisorption energy values for the NO_2 adsorption on the Sn-doped ZnO surface were −0.438 eV and −1.105 eV, respectively. These rates were relatively higher than those of the NO_2 adsorbed on the bare ZnO surface (see Table 1). Furthermore, it was found that the E_{ads} of the NH_3 molecule was −0.187 eV on the Sn-doped ZnO (101) surface, which was less than the E_{ads} value on the undoped surface.

The current findings revealed that the NO_2 molecule adsorption was more favorable on the doped surface than the NH_3 adsorption. The magnitude of the adsorption strength for NH_3 gas declines declined with Sn doping, whereas the interaction of the NO_2 molecule enhances. This indicates that NO_2 exhibited a stronger adsorption strength on the Sn-doped ZnO surface than NH_3. However, the NH_3 adsorption was more preferential than that of NO_2 on the bare ZnO (101) surface. This was also shown by the bond length interaction between the N atom (NO_2 and NH_3) and the surface atoms (Zn and Sn). This implies that the Sn-doped ZnO surface had a lower attraction of NH_3 gas while enhancing the stronger attraction of the NO_2 molecule. Previous work by Mhlongo et al. [31] demonstrated that, due to the high quantity of donor defects, the undoped ZnO-based surface responded to NH_3 gas more strongly than the doped ZnO, although transition-metal-doped sensors had faster responses and recovery periods than undoped ZnO.

3.3. Electronic Properties

Fundamentally, comprehending the classification of materials into the three groups of metals, semiconductors, and insulators depends on a system's electronic properties. The width of the energy band gap between the conduction band (CB) and the valence band (VB) establishes the kind of material. Using the lattice parameters a = b = c = 4.625 Å, the band energy for bulk ZnO was estimated and found to be 0.597 eV, which was lower than the empirically reported value [32]. As it is well-known that the DFT calculations underestimate the lowest unoccupied level, this is a common issue with the band gap of semiconductors. However, this drawback had no impact on the examination of electronic structure in our work. When the findings of the gas molecules adsorbed on the ZnO surface were compared using the same system and calculation method, this calculation error could be disregarded.

The measured lattice parameters and the required high symmetry directions of the matching irreducible Brillouin zone were used to optimize the clean ZnO (101) surface.

The calculated band structure revealed a direct energy band gap of 0.957 eV, as shown in Figure 3, which was located at the gamma (G) point. This value was higher than that of the bulk structure and indicates that the probability of distribution of the electrons was the greatest on the surface, i.e., the electron was constrained near the surface. The valence band of pure (101) ZnO surface, as seen from the density of states (DOS), had two peaks between 0 and 6.5 eV as well as between 15.9 and 17.0 eV. Doping (101) ZnO with Sn caused modifications in the electronic structure, as evidenced by the increase in the energy band gap from 0.957 to 1.03 eV and the addition of new peaks at about 20 eV in the DOS electronic structure.
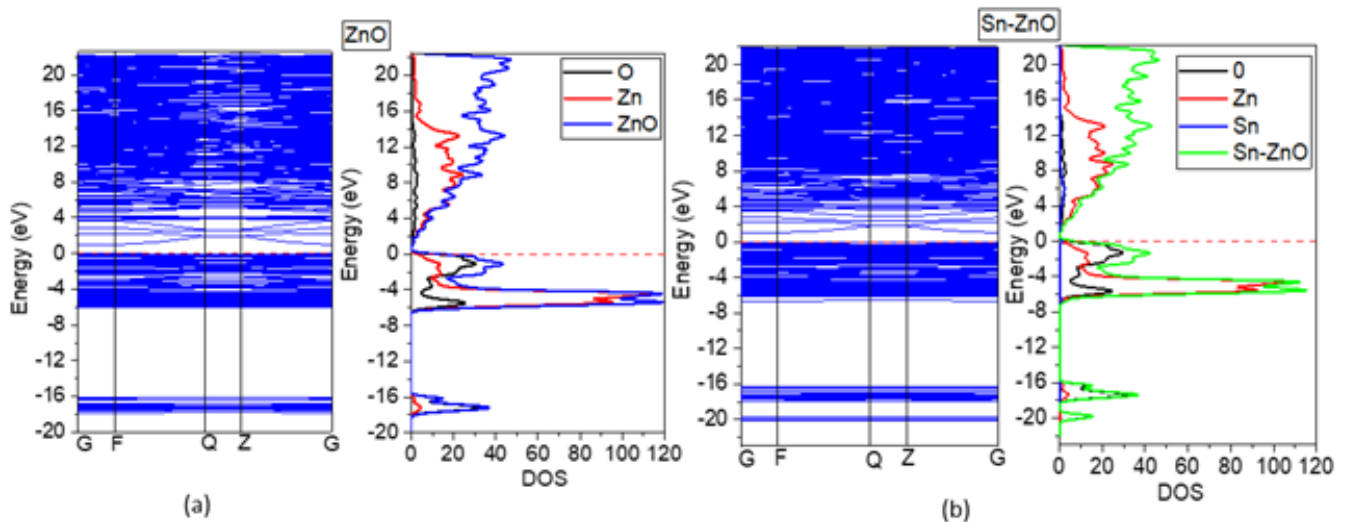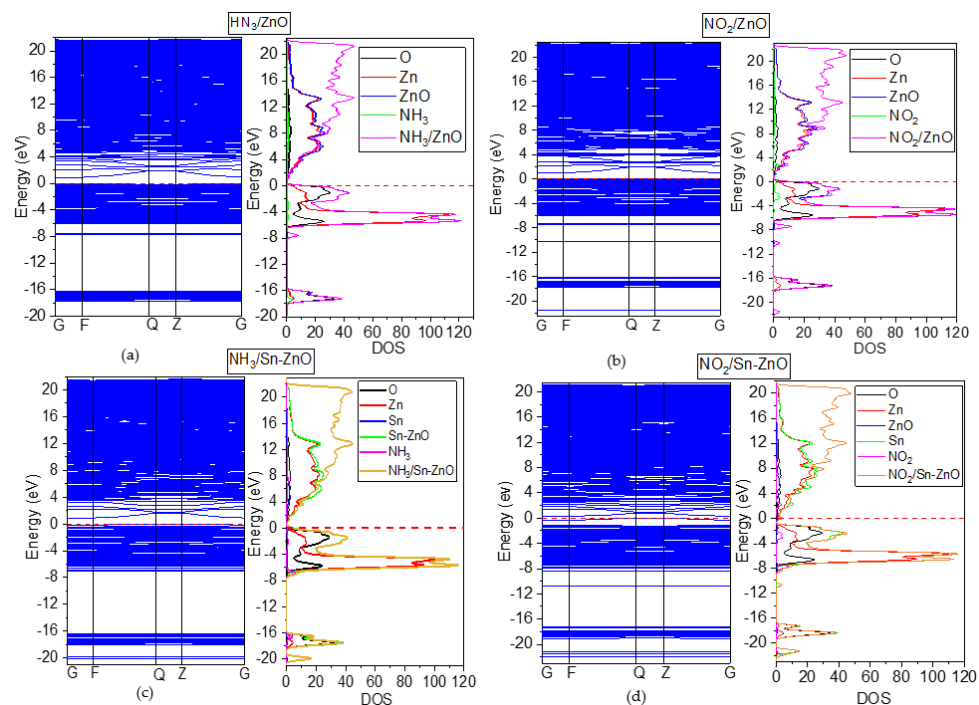

Figure 3. Band structures and DOS plots for (**a**) pure ZnO and (**b**) Sn−doped ZnO (101) surfaces.

Figure 4a–d show the electronic characteristics of NO_2 and NH_3 physisorption on ZnO (101) and Sn-doped ZnO (101) surfaces, where both NO_2 and NH_3 were adsorbed via a Van der Waals interaction to either Zn or Sn on the surface. The computed band gap values for NH_3/ZnO (101), NO_2/ZnO (101), NH_3/Sn-doped ZnO (101), and NO_2/Sn-doped ZnO (101) surfaces were 0.945 eV, 0.766 eV, 1.075 eV, and 0.634 eV, respectively. The predicted band gaps for the NO_2 adoption in both Sn-doped ZnO (101) and ZnO (101) surfaces were lower than the clean ZnO (101) surface, whereas the band gaps for the adsorbed NH_3 were larger. It was also discovered that the Fermi level of the NO_2/Sn-doped ZnO (101) surface introduced new states, resulting in the migration of both the conduction and valence bands, transforming the system from a p-type to an n-type semiconductor. DOS demonstrated the presence of molecular states in VB for all the structures, as seen by the creation of extra peaks near the bottom of the VB between −7 and 24 eV.

The band structures and DOS of NO_2 and NH_3 adsorbed on either the ZnO (101) or Sn-doped ZnO (101) surface through a chemical interaction are shown in Figure 5a–d. For NH_3/ZnO (101), NO_2/ZnO (101), NH_3/Sn-doped ZnO (101), and NO_2/Sn-ZnO (101), the calculated band-gap values were 0.937 eV, 0.991 eV, 0.911 eV, and 0.733 eV, respectively. For physisorption, NH_3/ZnO (101) and NH_3/Sn-doped ZnO (101) had larger band gaps than their equivalents, while NO_2/ZnO (101) and NO_2/Sn-doped ZnO (101) had band gaps lower than those obtained via chemisorption. This demonstrates that chemisorption and physisorption mechanisms had distinct effects on the band-gap values. However, we also made a similar observation on Fermi energy for NO_2/Sn-doped ZnO (101), where we noticed the emergence of new states at the bottom of the conduction band that overlapped the Fermi energy in the direction of the valence band, changing the system from a p-type to an n-type semiconductor. The emergence of additional peaks near the bottom of the VB between −7 and 24 eV in the case of DOS showed comparable observations to those in the case of chemisorbed mechanism, where we found the presence of molecular states in VB for all the structures.
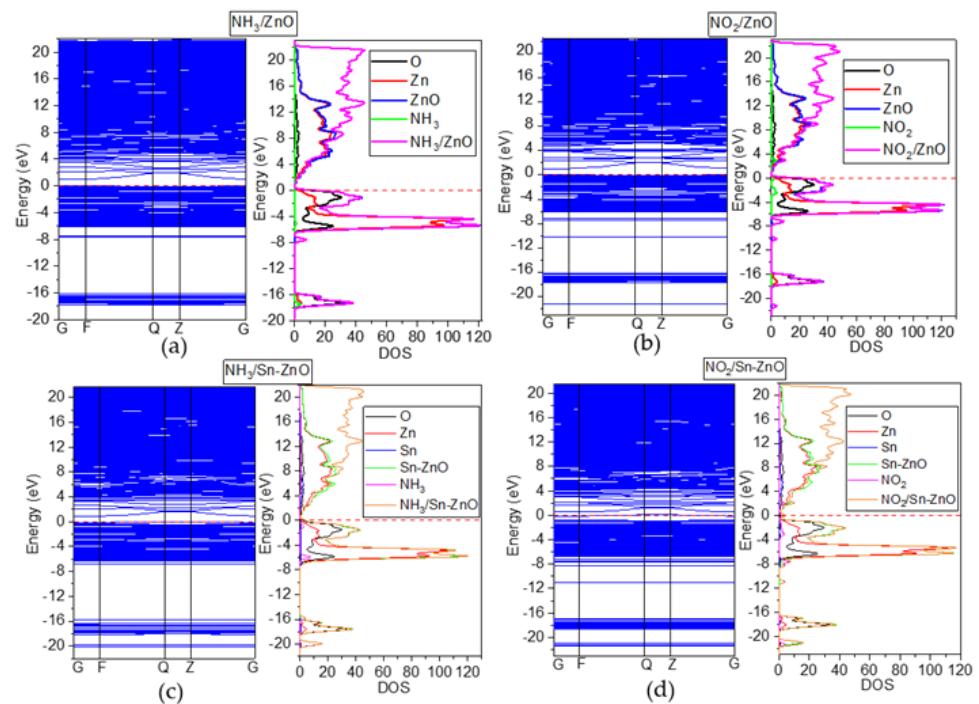
Figure 4. Band structures and DOS plots for physisorbed (**a**) NH_3/ZnO (101), (**b**) $NH_3/Sn-$doped ZnO (101), (**c**) NO_2/ZnO (101), and (**d**) $NO_2/Sn-$doped ZnO (101) surfaces.

Figure 5. Band structures and DOS plots for chemisorbed (**a**) NH_3/ZnO (101), (**b**) $NH_3/Sn-$doped ZnO (101), (**c**) NO_2/ZnO (101), and (**d**) $NO_2/Sn-$doped ZnO (101) surface.
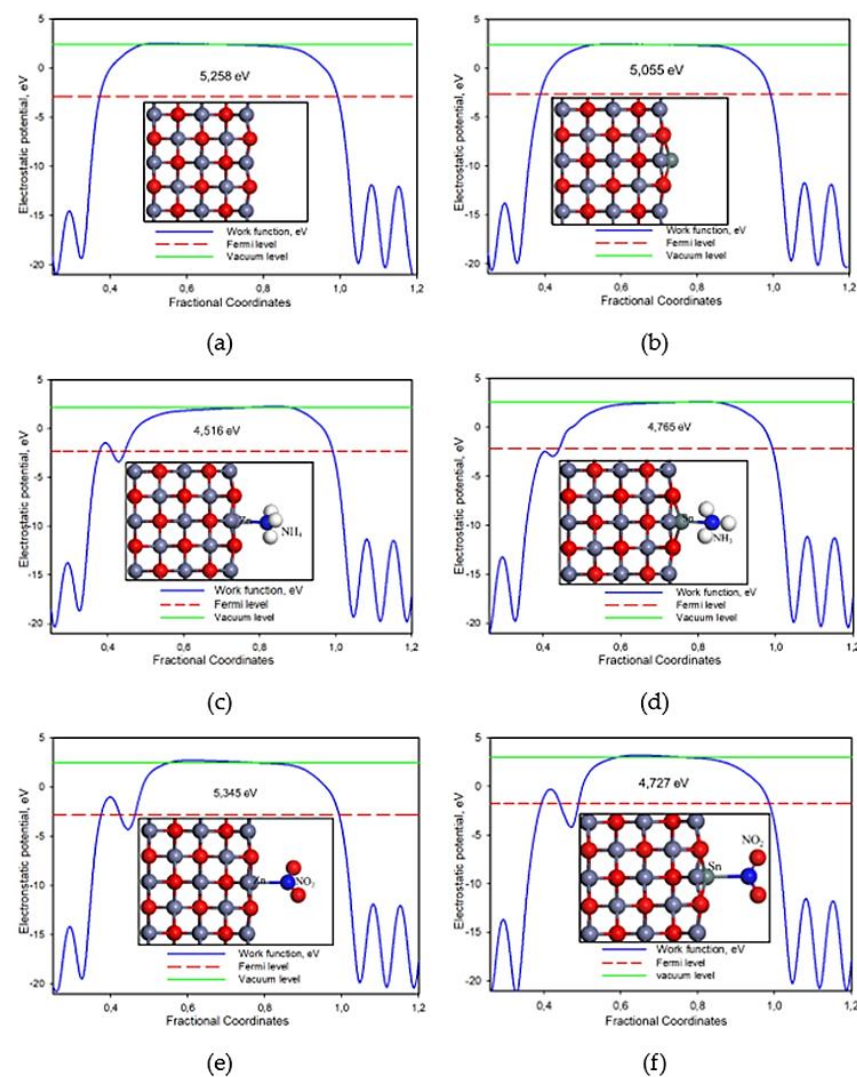
3.4. Work Function

The minimal amount of energy necessary to remove or extract an electron from a crystal surface in vacuum is known as the work function, which is commonly referred to as electrostatic potential. This is the most fundamental crystal solid surface parameter

for understanding a wide range of structural, physical, and chemical surface conditions. The electrostatic potential can be expressed as follows:

$$\Phi = E_{vac} - E_F \tag{2}$$

where E_{vac} and E_F represent the electrostatic potential energy of the vacuum and Fermi energy levels, respectively. In an adsorption system, the work function also plays a significant role in understanding the atomic interaction [33]. Figure 6 presents the work function plots for pure ZnO, Sn-doped ZnO, NH$_3$/ZnO, NO$_2$/ZnO, NH$_3$/Sn-doped ZnO, and NO$_2$/Sn-doped ZnO (101) surfaces. It appears that the work function of various surfaces significantly varied since it depended on the crystallographic orientation of the surface in most cases. The calculated work function of the ZnO (101) surface was 5.258 eV, which was comparable to the experiment work function value ranging from 5.4 to 6.5 eV [34]. It was observed that the computed work function (5.055 eV) of the Sn-doped ZnO (101) surface had a numerical value substantially smaller than that of the pure ZnO (101) surface. The value of the surface work function was reduced by 0.203 eV, compared with that of the undoped ZnO (101) surface; this is due to the charge rearrangement of electrons and ions at the surface. A surface with a lower work function easily transfers the electronic charge to any adsorbate with higher electronegativity, resulting in ionic bonding [35].

Figure 6. Work function plots for pure and adsorbed surfaces (**a**) pure ZnO (101), (**b**) Sn−doped ZnO, (**c**) NH$_3$/ZnO (101), (**d**) NO$_2$/ZnO (101), (**e**) NH$_3$/Sn−doped ZnO (101), and (**f**) NO$_2$/Sn-doped ZnO (101).

Furthermore, Figure 6 shows that the adsorption of NH_3 and NO_2 molecules changed the value of the work function compared with the pure and doped surfaces, indicating electron charge transfer. The adsorption of NH_3 and NO_2 on the surface of ZnO increased the value of the work function by 0.742 and 0.087 eV, respectively. The NH_3 molecule enhanced the surface work function larger than NO_2, which corresponded to a stronger adsorption energy strength. However, it was noted that adsorption on the Sn-doped ZnO surface reduced the surface work function. Previous researchers suggested that the induced work function is caused by a dipole involving the negative charge of the molecule [36].

3.5. Charge Density Distribution

The charge density distribution plots were examined in order to learn more about the nature of chemical bonding. The electronic hybridization between the molecule's orbital and the surface, as well as the molecule's adsorption and contact with the surface, caused the redistribution of charge density. Importantly, one of the attributes that facilitate the analysis of a chemical interaction is the changing density. It should be mentioned that charge density is influenced by crystal structure and can be used to comprehend a material's electrical properties. The charge density distribution for the current system was described as follows:

$$\Delta\rho_{system} = \rho_{mol/surf} - \rho_{surf} - \rho_{mol} \tag{3}$$

where $\rho_{mol\text{-}surf}$ is the charge density of the adsorbed surface, while ρ_{surf} and ρ_{mol} refer to the charge density for the pure surface and molecule, respectively. Figure 7 shows a 2D plot of the electronic density difference between the ZnO (101) and Sn-doped ZnO (101) surfaces. An electron-enriched ($-q$) area is shown by the blue region, while electron deduction is presented by the red regions. The plot of the electron charge difference presents a large blue isosurface on the O atom, while the red section is seen on both Zn and Sn atoms. This agrees with the Mulliken atomic charge values presented in Figure 7c,d.
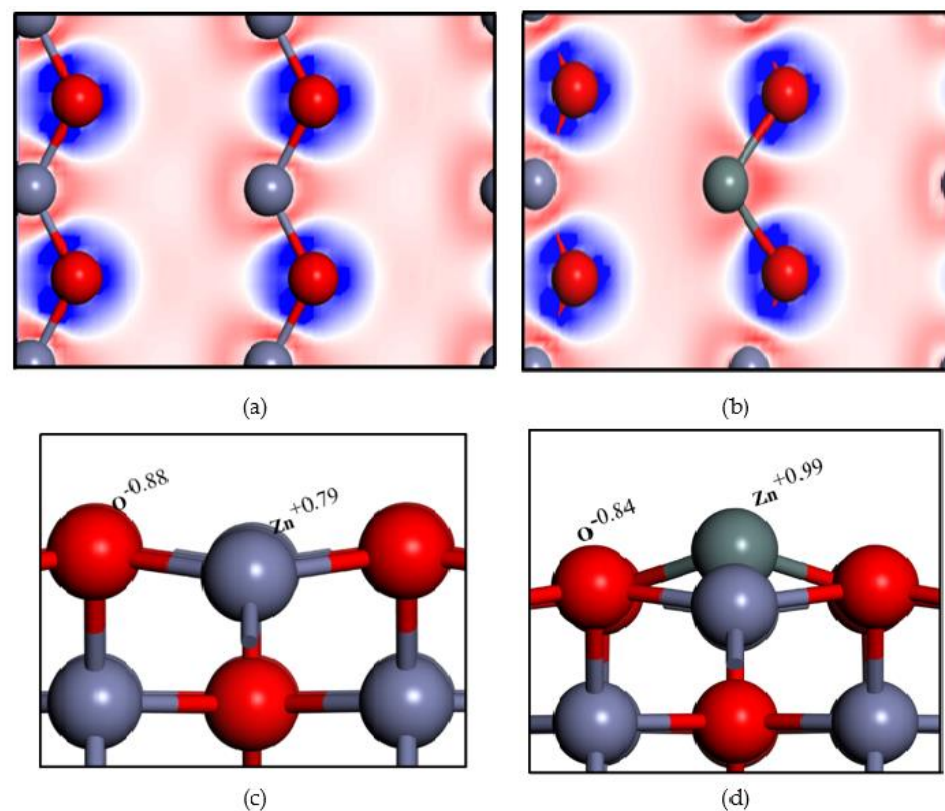
Figure 7. Electrons and charge distribution plots for (**a**,**c**) ZnO (101) surface and (**b**,**d**) Sn−doped ZnO (101) surfaces, respectively. Red–blue scale (isosurface range −0.14; +0.14).

Figure 8 presents the charge density distribution for NH_3/ZnO (101), NH_3/Sn-doped ZnO (101), NO_2/ZnO (101), and NO_2/Sn-doped ZnO (101) surfaces. As described in Equation 3, the charge density difference was calculated by subtracting the charge density of the pure or doped surface from that of the single (NH_3 and NO_2) molecule. The magnitude of the charges is represented by different colored regions, with yellow indicating depletion and blue indicating accumulation. The charges were primarily localized on the N-Zn and N-Sn bonding, according to the 3D isosurfaces of the charge redistribution, as seen in Figure 8. The figure shows that the charge distribution in the isosurface region significantly differed from one model to the other. A wide isosurface region indicates a greater adsorption strength and suggests an increased charge transfer rate. As shown in Figure 8a, a large isosurface region was observed on the NH_3/ZnO (101) adsorption, while a smaller volume was seen for the NO_2 adsorption. This is similar to the adsorption energy strength reported in Table 1 and the larger value of the work function in Figure 6.
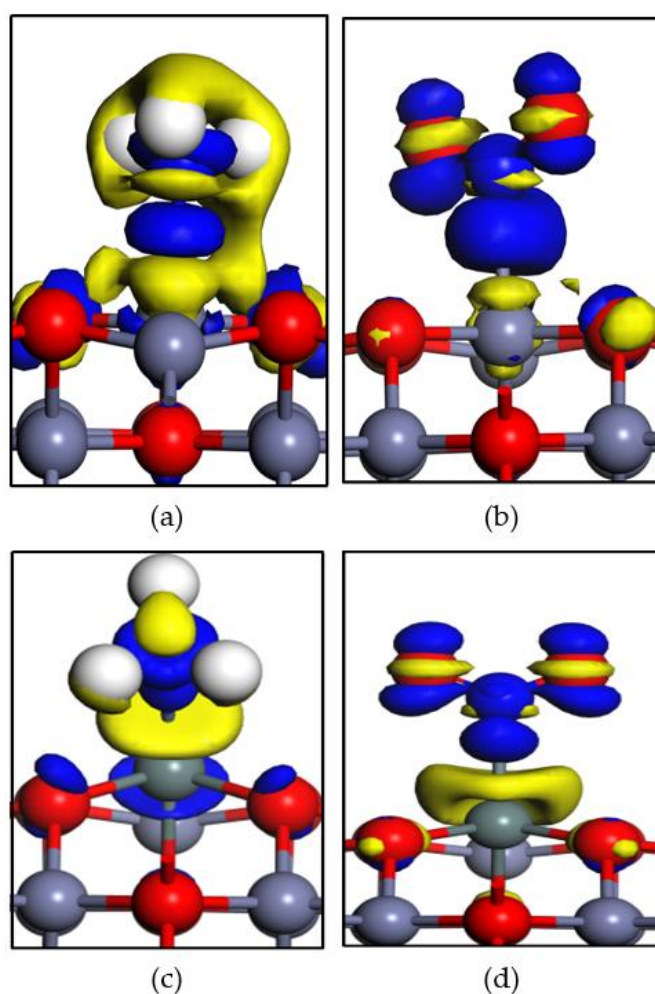
Figure 8. Charge density difference for (**a**) NH_3/ZnO (101) surface, (**b**) NO_2/ZnO (101), (**c**) $NH_3/Sn-$doped ZnO (101), and (**d**) $NO_2/Sn-$doped ZnO (101) surface. The blue and yellow regions show electron accumulation and depletion, respectively.

Furthermore, the charge density distribution plot for the NH_3/ZnO (101) adsorption showed a covalent character, while for NO_2/ZnO (101), NO_2/Sn-doped ZnO (101), NH_3/Sn-doped ZnO surfaces, it showed the ionic character of the bonding. The yellow isosurface was discovered to be between the interactions of Zn-N and Sn-N (both N atoms from NH_3 and NO_2), indicating electron depletion from the surface atom. This means that the molecules serve as electron acceptors. A directional bonding of spherical shape was observed, which indicates ionic bonding. This was also reported by Tshwane et al. [36]

on the adsorption of halogen ions and molecules. Furthermore, the yellow region for the NO_2/Sn-doped ZnO surface was larger than that observed on the NH_3/Sn-doped ZnO surface. This is due to the larger negative and stronger adsorption energy strength presented in Table 1.

4. Conclusions

In conclusion, the adsorption mechanisms of NH_3 and NO_2 molecules on ZnO and Sn-doped ZnO (101) surfaces were successfully investigated using density functional theory. The study considered both the chemisorption and physisorption phenomena. The calculated adsorption energy values were found to be negative, implying that the adsorption mechanism is thermodynamically favorable. It was discovered that both molecules adsorb on the surface via chemisorption rather than physisorption, which is due to the stronger interaction of N and Zn or Sn atoms. The adsorption strength of NH_3 on the ZnO surface was found to be more stable, whereas the NO_2 adsorption configuration on the Sn-doped ZnO surface was preferred. The relatively larger negative E_{ads} value indicated a stronger adsorbing strength. Furthermore, the adsorption of both molecules induced the charge density redistribution and changed the surface work function. This analysis revealed the charge accumulation and depletion patterns at the interface. Moreover, the results revealed that the surface work function increased on the doped ZnO surface while decreasing on the undoped ZnO surface.

Author Contributions: Conceptualization, R.S.D., D.M.T. and K.S.; methodology, R.S.D., D.M.T., R.M. and R.R.M.; software, R.S.D., D.M.T., R.M. and R.R.M.; validation, R.M., R.R.M. and N.E.M.; formal analysis, R.S.D. and D.M.T.; investigation, R.S.D. and D.M.T.; resources, R.M. and R.R.M.; data curation, R.S.D. and D.M.T.; writing—original draft preparation, R.S.D., D.M.T. and K.S.; writing—review and editing, R.S.D., D.M.T., K.S., R.M., R.R.M. and N.E.M.; visualization, R.S.D. and D.M.T.; supervision, R.M., R.R.M. and N.E.M.; project administration, R.S.D.; funding acquisition, R.R.M. and N.E.M. All authors have read and agreed to the published version of the manuscript.

Institutional Review Board Statement: Not applicable.

Informed Consent Statement: Not applicable.

Data Availability Statement: Not applicable.

Conflicts of Interest: The authors declare no conflict of interest.

References

1. Yong, Y.; Ren, F.; Zhao, Z.; Gao, R.; Hu, S.; Zhou, Q.; Kuang, Y. Highly enhanced NH3-sensing performance of BC6N monolayer with single vacancy and Stone-Wales defects: A DFT study. *Appl. Surf. Sci.* **2021**, *551*, 149383. [CrossRef]
2. Ou, J.Z.; Ge, W.; Carey, B.; Daeneke, T.; Rotbart, A.; Shan, W.; Wang, Y.; Fu, Z.; Chrimes, A.F.; Wlodarski, W. Physisorption-based charge transfer in two-dimensional SnS2 for selective and reversible NO2 gas sensing. *ACS Nano* **2015**, *9*, 10313–10323. [CrossRef] [PubMed]
3. Ji, H.; Zeng, W.; Li, Y. Gas sensing mechanisms of metal oxide semiconductors: A focus review. *Nanoscale* **2019**, *11*, 22664–22684. [CrossRef] [PubMed]
4. Mahajan, S.; Jagtap, S. Metal-oxide semiconductors for carbon monoxide (CO) gas sensing: A review. *Appl. Mater. Today* **2020**, *18*, 100483. [CrossRef]
5. Mirzaei, A.; Kim, S.S.; Kim, H.W. Resistance-based H2S gas sensors using metal oxide nanostructures: A review of recent advances. *J. Hazard. Mater.* **2018**, *357*, 314–331. [CrossRef] [PubMed]
6. Mirzaei, A.; Lee, J.; Majhi, S.M.; Weber, M.; Bechelany, M.; Kim, H.W.; Kim, S.S. Resistive gas sensors based on metal-oxide nanowires. *J. Appl. Phys.* **2019**, *126*, 241102. [CrossRef]
7. Gupta, S.K.; Joshi, A.; Kaur, M. Development of gas sensors using ZnO nanostructures. *J. Chem. Sci.* **2010**, *122*, 57–62. [CrossRef]
8. Shingange, K.; Mhlongo, G.H.; Motaung, D.E.; Ntwaeaborwa, O.M. Tailoring the sensing properties of microwave assisted grown ZnO nanorods: Effect of irradiation time on luminescence and magnetic behavior. *J. Alloys Compd.* **2016**, *657*, 917–926. [CrossRef]

9. Onkar, S.G.; Nagdeote, S.B.; Wadatkar, A.S.; Kharat, P.B. Gas sensing behavior of ZnO thick film sensor towards H2S, NH3, LPG and CO$_2$. *J. Phys. Conf. Ser.* **2020**, *1644*, 012060. [CrossRef]

10. Choi, M.S.; Kim, M.Y.; Mirzaei, A.; Kim, H.; Kim, S.; Baek, S.; Chun, D.W.; Jin, C.; Lee, K.H. Selective, sensitive, and stable NO$_2$ gas sensor based on porous ZnO nanosheets. *Appl. Surf. Sci.* **2021**, *568*, 150910. [CrossRef]

11. Wei, S.; Wang, S.; Zhang, Y.; Zhou, M. Different morphologies of ZnO and their ethanol sensing property. *Sens. Actuators B Chem.* **2014**, *192*, 480–487. [CrossRef]

12. Zhu, L.; Zeng, W. Room-temperature gas sensing of ZnO-based gas sensor: A review. *Sens. Actuators A Phys.* **2017**, *267*, 242–261. [CrossRef]

13. Kang, Y.; Yu, F.; Zhang, L.; Wang, W.; Chen, L.; Li, Y. Review of ZnO-based nanomaterials in gas sensors. *Solid State Ion.* **2021**, *360*, 115544. [CrossRef]

14. Shingange, K.; Swart, H.C.; Mhlongo, G.H. Au functionalized ZnO rose-like hierarchical structures and their enhanced NO$_2$ sensing performance. *Phys. B Condens. Matter* **2018**, *535*, 216–220. [CrossRef]

15. Yu, A.; Li, Z.; Yi, J. Selective detection of parts-per-billion H2S with Pt-decorated ZnO nanorods. *Sens. Actuators B Chem.* **2021**, *333*, 129545. [CrossRef]

16. Kolhe, P.S.; Shinde, A.B.; Kulkarni, S.G.; Maiti, N.; Koinkar, P.M.; Sonawane, K.M. Gas sensing performance of Al doped ZnO thin film for H$_2$S detection. *J. Alloys Compd.* **2018**, *748*, 6–11. [CrossRef]

17. Chu, Y.; Young, S.; Ji, L.; Chu, T.; Lam, K.; Hsiao, Y.; Tang, I.; Kuo, T. Characteristics of gas sensors based on Co-doped ZnO nanorod arrays. *J. Electrochem. Soc.* **2020**, *167*, 117503. [CrossRef]

18. Sharma, B.; Sharma, A.; Joshi, M.; Myung, J. Sputtered SnO$_2$/ZnO heterostructures for improved NO$_2$ gas sensing properties. *Chemosensors* **2020**, *8*, 67. [CrossRef]

19. Yang, X.; Zhang, S.; Zhao, L.; Sun, P.; Wang, T.; Liu, F.; Yan, X.; Gao, Y.; Liang, X.; Zhang, S. One step synthesis of branched SnO$_2$/ZnO heterostructures and their enhanced gas-sensing properties. *Sens. Actuators B Chem.* **2019**, *281*, 415–423. [CrossRef]

20. Patil, V.L.; Dalavi, D.S.; Dhavale, S.B.; Tarwal, N.L.; Vanalakar, S.A.; Kalekar, A.S.; Kim, J.H.; Patil, P.S. NO$_2$ gas sensing properties of chemically grown Al doped ZnO nanorods. *Sens. Actuators A Phys.* **2022**, *340*, 113546. [CrossRef]

21. Zhao, S.; Shen, Y.; Li, A.; Chen, Y.; Gao, S.; Liu, W.; Wei, D. Effects of rare earth elements doping on gas sensing properties of ZnO nanowires. *Ceram. Int.* **2021**, *47*, 24218–24226. [CrossRef]

22. Qu, Y.; Ding, J.; Fu, H.; Peng, J.; Chen, H. Adsorption of CO, NO, and NH$_3$ on ZnO monolayer decorated with noble. *Appl. Surf. Sci.* **2020**, *508*, 145202. [CrossRef]

23. Liangruksa, M.; Laomettachit, T.; Siriwong, C. Enhancing gas sensing properties of novel palladium-decorated zinc oxide surface: A first-principles study. *Mater. Res. Express* **2021**, *8*, 045004. [CrossRef]

24. Prades, J.D.; Cirera, A.; Morante, J.R.; Pruneda, J.M.; Ordejón, P. Ab initio study of NO$_x$ compounds adsorption on SnO2 surface. *Sens. Actuators B Chem.* **2007**, *126*, 62–67. [CrossRef]

25. Cheng, Q.; Li, Y.; Qiao, X.; Zhao, Y.; Zhang, Q.; Ju, Y.; Shi, Y. Molecular modelling of ammonia gas adsorption onto the Kaolonite surfaces with DFT study. *Minerals* **2020**, *10*, 46. [CrossRef]

26. Zhu, B.; Fang, Q.; Sun, Y.; Yin, S.; Li, G.; Zi, Z. Adsorption properties of NO, NH$_3$, and O$_2$ over beta MnO$_2$ (110) surface. *J. Mater. Sci.* **2018**, *53*, 11500–11511. [CrossRef]

27. Supatutkul, C.; Pramchu, S.; Jarroenjittichai, A.P.; Laosiritaworn, Y. Density functional theory investigation of surface defects in Sn-doped ZnO. *Surf. Coat. Technol.* **2016**, *298*, 53–57. [CrossRef]

28. Segall, M.D.; Lindan, P.J.D.; Probert, M.J.; Pickard, C.J.; Hasnip, P.J.; Clark, S.J.; Payne, M.C. First-principles simulation: Ideas, illustrations and the CASTEP code. *J. Phys. Condens. Matter* **2002**, *14*, 2717–2744. [CrossRef]

29. Perdew, J.P.; Burke, K.; Ernzerhof, M. Generalized gradient approximation made simple. *Phys. Rev. Lett.* **1996**, *77*, 3865–3868. [CrossRef]

30. Monkhorst, H.J.; Pack, J.D. Special points for Brillouin-zone integrations. *Phys. Rev. B* **1976**, *13*, 5188–5192. [CrossRef]

31. Mhlongo, G.H.; Shingange, K.; Tshabalala, Z.P.; Dhonge, B.P.; Mahmoud, F.A.; Mwakikunga, B.W.; Motaung, D.E. Room temperature ferromagnetism and gas sensing in ZnO nanostructures: Influence of intrinsic defects and Mn, Co, Cu doping. *Appl. Surf. Sci.* **2016**, *390*, 804–815. [CrossRef]

32. Zhang, Y.H.; Li, Y.L.; Gong, F.L.; Xie, K.F.; Liu, M.; Zhang, H.L.; Fang, S.M. Al doped narcissus-like ZnO for enhanced NO$_2$ sensing performance: An experimental and DFT investigation. *Sens. Actuators B Chem.* **2020**, *305*, 127489. [CrossRef]

33. Guo, G.; Wu, H.; Liu, J.; Zhang, Y.; Xie, Z. Tuning the electronic and magnetic properties of monolayer germanium triphosphide adsorbed by halogen atoms: Insights from first principles study. *Physica E* **2021**, *127*, 114537. [CrossRef]

34. Schlesinger, R.; Xu, Y.; Hofmann, O.T.; Winkler, S.; Frisch, J.; Niederhausen, J.; Vollmer, A.; Blumstengel, S.; Henneberger, F.; Rinke, P.; et al. Controlling the work function of ZnO and the energy-level alignment at the interface to organic semiconductors with a molecular electron acceptor. *Phys. Rev. B* **2013**, *87*, 155311. [CrossRef]

35. Roman, T.; Gossenberger, F.; Forster-Tonigold, K.; Groß, A. Halide adsorption on close-packed metal electrodes. *Phys. Chem. Chem. Phys.* **2014**, *16*, 13630–13634. [CrossRef] [PubMed]

36. Tshwane, D.M.; Modiba, R.; Govender, G.; Ngoepe, P.E.; Chauke, H.R. The adsorption of halogen molecules on Ti (110) surface. *J. Mater. Res.* **2021**, *36*, 592–601. [CrossRef]